High-Fidelity Numerical Analysis of Per-Rev-Type Inlet Distortion Transfer in Multistage Fans—Part II: Entire Component Simulation and Investigation

Jixian Yao
GE Global Research,
One Research Circle,
Niskayuna, NY 12309

Steven E. Gorrell
Department of Mechanical Engineering,
Brigham Young University,
435 CTB, Provo, UT 84602

Aspi R. Wadia
GE Aviation,
30 Merchant Street, P20,
Cincinnati, OH 45215

Part I of this paper validated the ability of the unsteady Reynolds-Averaged Navier-Stokes (RANS) solver PTURBO *to accurately simulate distortion transfer and generation through selected blade rows of two multistage fans. In this part, unsteady RANS calculations were successfully applied to predict the 1/rev inlet total pressure distortion transfer in the entirety of two differently designed multistage fans. This paper demonstrates that high-fidelity computational fluid dynamics (CFD) can be used early in the design process for verification purposes before hardware is built and can be used to reduce the number of distortion tests, hence reducing engine development cost. The unsteady RANS code* PTURBO *demonstrated remarkable agreement with the data, accurately capturing both the magnitude and the profile of total pressure and total temperature measurements. Detailed analysis of the flow physics identified from the CFD results has led to a thorough understanding of the total temperature distortion generation and transfer mechanism, especially for the spatial phase difference of total pressure and total temperature profiles. The analysis illustrates that the static parameters are more revealing than their stagnation counterpart and that pressure and temperature rise are more revealing while the pressure and temperature ratio could be misleading. The last stage is effectively throttled by the inlet distortion even though the overall engine throttle remains unchanged. The total temperature distortion generally grows as flow passes through the fan stages.* [DOI: 10.1115/1.3148479]

1 Introduction

Unsteady Reynolds-Averaged Navier-Stokes (RANS) calculations were successfully applied to predict temperature distortion generation and transfer of total pressure distortion in response to 1/rev inlet total pressure distortion [1]. Validation with total pressure and total temperature experimental data showed that simulations predicted the proper magnitude and phase of distortion transfer and generation in the front block of one multistage fan and the rear block of another fan. Each of these fans consists of an inlet guide vane (IGV) and three stages, with engine test data to validate the CFD procedure.

As the capability of parallel computing and processor speed has steadily increased, numerical simulations play an increasingly important role in discovering the physics of unsteady flows in turbomachinery. High performance computing allows full annulus simulations to be obtained in an acceptable time frame to be of benefit to the engine design process.

Part I presented the motivation for this research and thoroughly reviewed the history and models used to understand and predict the impact of inlet distortion on stall margin. This high-fidelity CFD effort is unique in its attempt to evaluate the ability to model inlet distortion at a much higher fidelity level and to establish a capable prediction tool for distortion transfer and fan response characterization in multistage turbomachinery. With the CFD methodology and computational requirements defined in Part I resulting in a very successful validation, Part II builds on the initial high-fidelity CFD capability to model the entirety (three stages plus IGV) of two multistage fans subject to 1/rev inlet distortion.

Part II is focused on a higher fidelity understanding of distortion transfer and fan response besides the large-scale simulations. A full-range validation is carried out for the multistage CFD prediction, and the simulations are analyzed to understand the physics of temperature distortion generation and transfer. Accurate prediction of total temperature distortion is important as it affects the corrected speed for downstream rotors and flow capacity of stators. The level of induced temperature distortion entering the core compressor is also an important factor since the temperature distortion is usually amplified as the fan attenuates the pressure distortion. Analysis of the simulations from Part I [1] suggested that static temperature dominated the total temperature phasing. This alluded to the examination of the distortion profiles of both static pressure and density in Part I. Further investigation from the fan response perspective is carried out in this paper for the multistage environment for the underlying mechanism of distortion transfer.

The paper is divided into sections discussing the computational domain and boundary conditions, the full-range validation against engine test data, the mechanism of total temperature distortion generation, and the distortion transfer analysis.

2 Computational Domains and Boundary Conditions

This section describes the overall configuration of the two selected fans, the computational domains, and the boundary conditions used for the simulations. The flow solver chosen was the unsteady RANS code, PTURBO (see Part I), developed by Dr. Jenping Chen with support from NASA, Industry, and the DoD. Its

Contributed by the International Gas Turbine Institute of ASME for publication in the JOURNAL OF TURBOMACHINERY. Manuscript received September 9, 2008; final manuscript received January 28, 2009; published online May 6, 2010. Review conducted by David Wisler. Paper presented at the ASME Turbo Expo 2008: Land, Sea and Air (GT2008), Berlin, Germany, June 9–13, 2008.

Downloaded 28 May 2010 to 128.113.26.88. Redistribution subject to ASME license or copyright; see http://www.asme.org/terms/Terms_Use.cfm

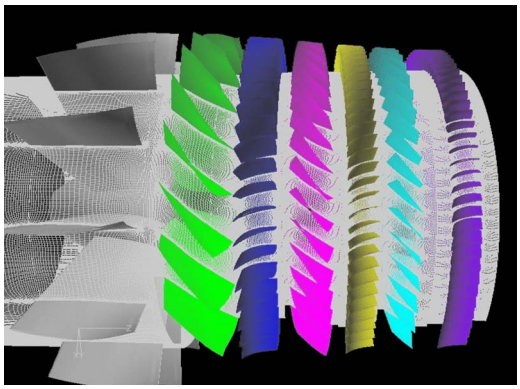

Fig. 1 Computational domain and grid of the first multistage fan (not drawn to scale)

solution algorithm is an implicit finite volume solver that incorporates Newton subiterations and a block-Jacobi relaxation scheme at each physical time step. It has a third-order accurate monotonic upstream-centered schemes for conservation laws (MUSCL)-type spatial discretization scheme coupled with a second-order accurate temporal discretization, which helps to improve flow resolution and minimize dispersion error. Turbulence modeling is accomplished via the NASA/CMOTT k-epsilon model specifically developed for turbomachinery flows. This code was modified by GE to accept distortion boundary conditions at inlet and exit boundaries. With predetermined load balancing, this flow solver has demonstrated high scalability and parallel efficiency.

2.1 First Multistage Fan. The first multistage fan consists of three stages with an IGV, as shown in Fig. 1. The computational domain consists of all seven blade rows, full annulus for each blade row. The blade counts and grid sizes for each passage of all the blade rows are listed in Table 1.

The IGV and the stator rows were properly clocked to match engine test setup. Boundary conditions were obtained from the engine inlet distortion test. The inlet total pressure was a stationary (in absolute frame of reference) 1/rev sinusoidal distribution in the fan circumference. There were no circumferential distortions of total temperature and inflow swirl. The peak-to-peak total pressure distortion at inlet was about 20% of the circumferential mean. Figure 2(a) shows the absolute total pressure distribution at inlet. The inlet boundary conditions were exactly the same as that used in Part I of this paper.

The exit boundary condition downstream of Stator-3 was more difficult to specify. The total pressure distortion was expected to be attenuated at fan exit but the static pressure there was not completely distortion-free. The engine test only had readings at hub and casing, with none in-between. The static pressure profile at this location was obtained from GE's data matched through-flow solution and was scaled to match the measurements from the hub and casing. The resulting exit static pressure distribution is

Table 1 Blade counts and grid sizes of the first multistage fan, 201×10^6 grid cells total (including halo cells)

Blade row	Blade count	Mesh size/passage ($\theta\times z\times r$)
IGV	13	$137\times145\times81$
Rotor-1	24	$97\times131\times81$
Stator-1	62	$49\times105\times81$
Rotor-2	46	$65\times109\times81$
Stator-2	94	$41\times101\times81$
Rotor-3	50	$65\times109\times81$
Stator-3	96	$41\times121\times81$

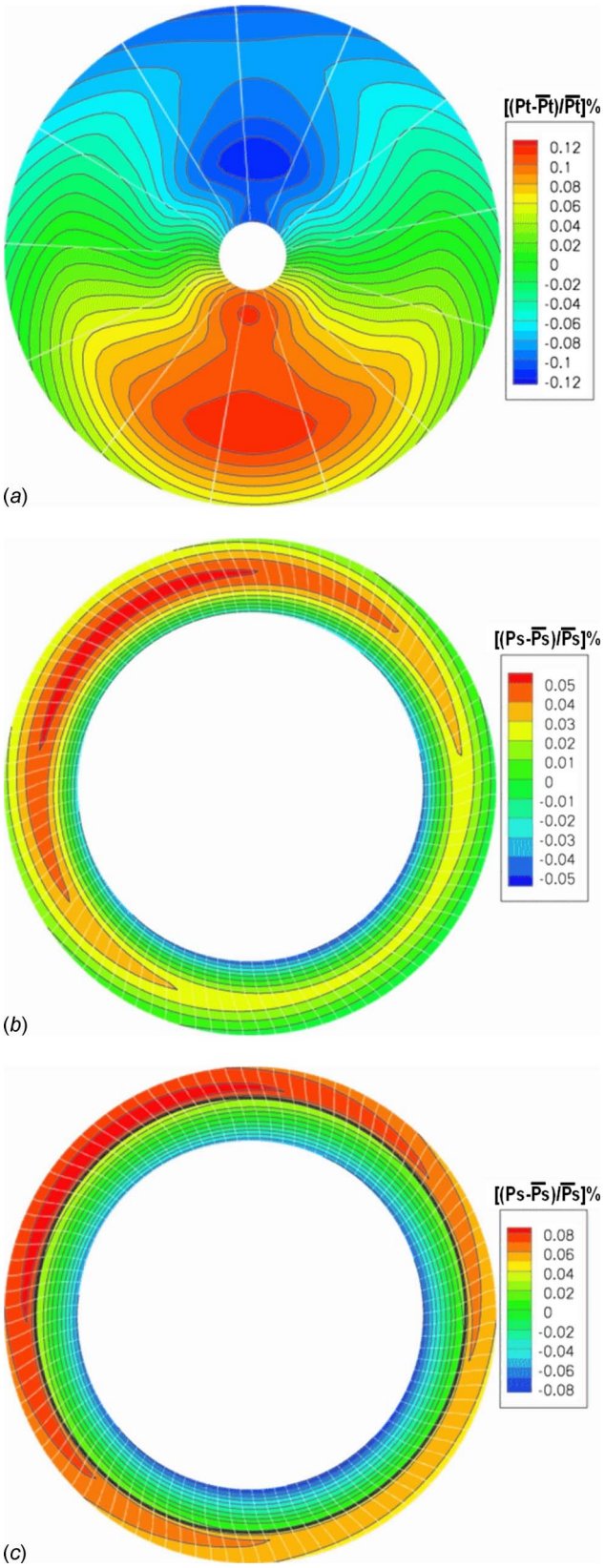

Fig. 2 Boundary conditions of the first multistage fan: 1/rev total pressure distortion at inlet (a) and the static pressure distribution at Stator-3 exit ((b) and (c)). $[(Pt-\bar{Pt})/\bar{Pt}]\%$ is plotted in (a), and $[(Ps-\bar{Ps})/\bar{Ps}]\%$ is plotted in (b) and (c).

Downloaded 28 May 2010 to 128.113.26.88. Redistribution subject to ASME license or copyright; see http://www.asme.org/terms/Terms_Use.cfm

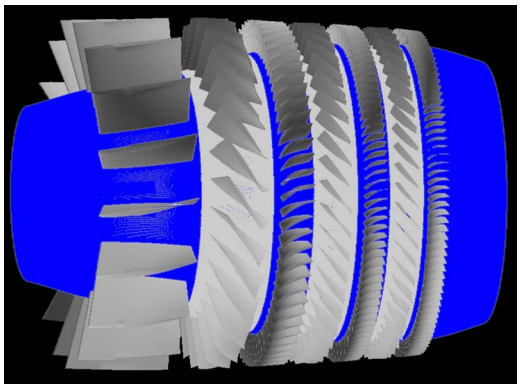

Fig. 3 Computational domain and grid of the second multistage fan (not drawn to scale)

shown in Fig. 2(*b*). This exit boundary condition corresponds to the operating condition at about 97% corrected speed on the operating line. Physical rotating speed is about 8788 rpm.

An additional near-stall operating condition for this fan was also simulated at the same speed. At this condition, additional measurement of static pressure at the engine splitter leading edge was used for the specification of the back pressure profile. The near-stall back pressure distribution is shown in Fig. 2(*c*).

2.2 Second Multistage Fan. The second multistage fan also consists of three stages with an IGV. This fan has a higher overall pressure ratio and has a different design philosophy than the first fan. Validation for both fans, therefore, would enhance our confidence toward the numerical prediction capability, in contrast to validating against another fan similar to the first one.

The entire second fan model is shown in Fig. 3. The computational domain consists of all seven blade rows, full annulus for each blade row. The blade counts and grid sizes for each passage of all the blade rows are listed in Table 2. The IGV and the stator rows were properly clocked to match engine test setup. The rotor rows were properly clocked as well to the specification of the engine test. The engine test used a distortion screen to produce the designed total pressure distortion pattern. The inlet boundary conditions were similar to that used for the first fan. A stationary (in absolute frame of reference) 1/rev sinusoidal distortion of total pressure was specified. Total temperature and flow angles were uniformly distributed in the circumference, but the radial profiles were retained. The peak-to-peak total pressure distortion at inlet was about 35% of the circumferential mean, which was significantly higher than the inlet distortion level of the first fan. Figure 4(*a*) shows the absolute total pressure distribution at inlet.

The exit boundary condition was determined using the same method described for the first fan. The exit location was set in-between the fan OGV and the leading edge of the splitter. The static pressure profile at this location was obtained from the data-matched through-flow solution and was scaled to match the measurements from the hub and casing. This exit boundary condition corresponds to the operating condition at about 100% corrected speed on the operating line. The physical rotating speed of this fan is about 12,000 rpm. The resulting exit boundary condition distribution is shown in Fig. 4(*b*).

Table 2 Blade counts and grid sizes of the second multistage fan, 313×10^6 grid cells total (including halo cells)

Blade row	Blade count	Mesh size/passage ($\theta\times z\times r$)
IGV	17	$97\times169\times81$
Rotor-1	28	$85\times129\times81$
Stator-1	68	$49\times113\times81$
Rotor-2	42	$65\times127\times81$
Stator-2	108	$49\times113\times81$
Rotor-3	50	$65\times127\times81$
Stator-3	118	$49\times169\times81$

2.3 Nonuniform Boundary Condition Specification. The distortion screens for both fans were designed to produce sinusoidal total pressure distortions, so a sinusoidal function was fitted through the inflow total pressure data using Eq. (1) at various immersions. As a result, the radial profiles of the circumferentially averaged total pressure, the amplitude, and the phase angle of the total pressure were specified to the CFD flow solver. The CFD flow solver then interpolates the boundary conditions onto the computational mesh at inlet to the fans. The same method was used for the back pressure specification.

$$Pt = Pt_{\text{ave}} \cdot (1 + \text{amp}_{\_Pt} \cos(\text{phase}_{\_Pt} + \theta)) \tag{1}$$

3 Validation

This section provides the full validation of the numerical simulations to both multistage fans. The validation is a fundamental and foremost effort for this research, and the focus is to validate

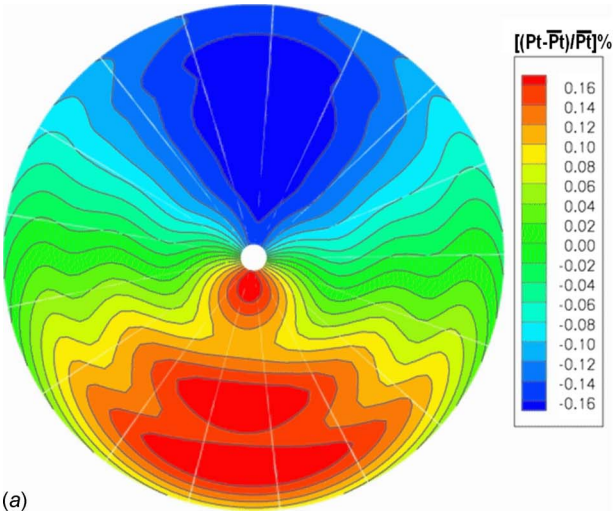

Fig. 4 Boundary conditions of the second multistage fan: 1/rev total pressure distortion at inlet (*a*) and the static pressure distribution at Stator-3 exit (*b*). $[(Pt-\bar{Pt})/\bar{Pt}]\%$ is plotted in (a) and $[(Ps-\bar{Ps})/\bar{Ps}]\%$ is plotted in (b).

Downloaded 28 May 2010 to 128.113.26.88. Redistribution subject to ASME license or copyright; see http://www.asme.org/terms/Terms_Use.cfm

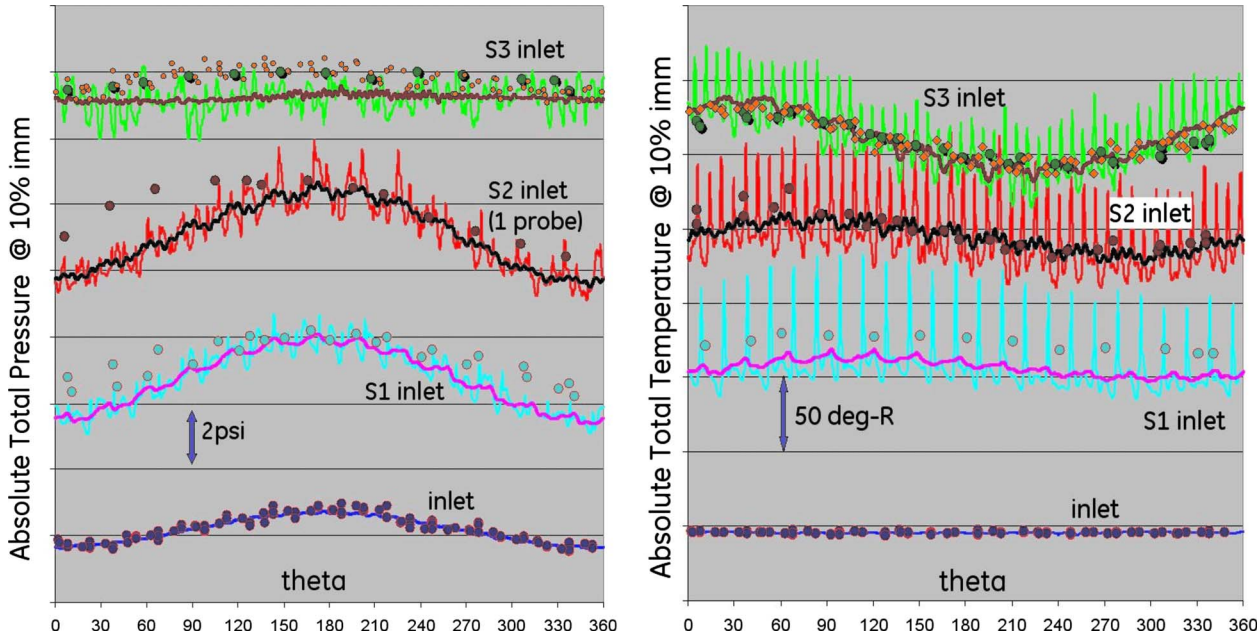

Fig. 5 Comparison of total pressure and total temperature profiles at about 10% immersion; first fan. Lines with rapid oscillation are the time instantaneous solution. Overlaid smoother lines are time-averaged solution. Solid symbols are measured data.

the general unsteady RANS capability instead of a particular flow solver. No parameters relating to numerical algorithms and turbulence models were varied to gain a better match to data. Even though the distortion transfer does have its requirement for CFD procedures, these procedures can be met by any well-written flow solvers in the unsteady RANS flow regime. For the flow solver information and initial validation, please refer to Part I of this paper [1].

3.1 Validation of the First Multistage Fan. Total pressure and total temperature measurements were available at various radial locations at the leading edge of all three vane rows and at the distortion screen located further upstream of the IGV. Comparisons of the CFD results against data are included in this section for all available total pressure and total temperature data. The CFD results are time averaged from the time-accurate calculations covering one rotor revolution which had 15,360 physical time steps. The time-average process is a simple trapezoidal averaging of time-resolved total pressure and total temperature.

Figures 5–9 compare the total pressure and total temperature at all five immersions. Time-averaged CFD results are shown with overlay of one time instantaneous solution to illustrate unsteady variations. Symbols represent steady-state data points. Not all

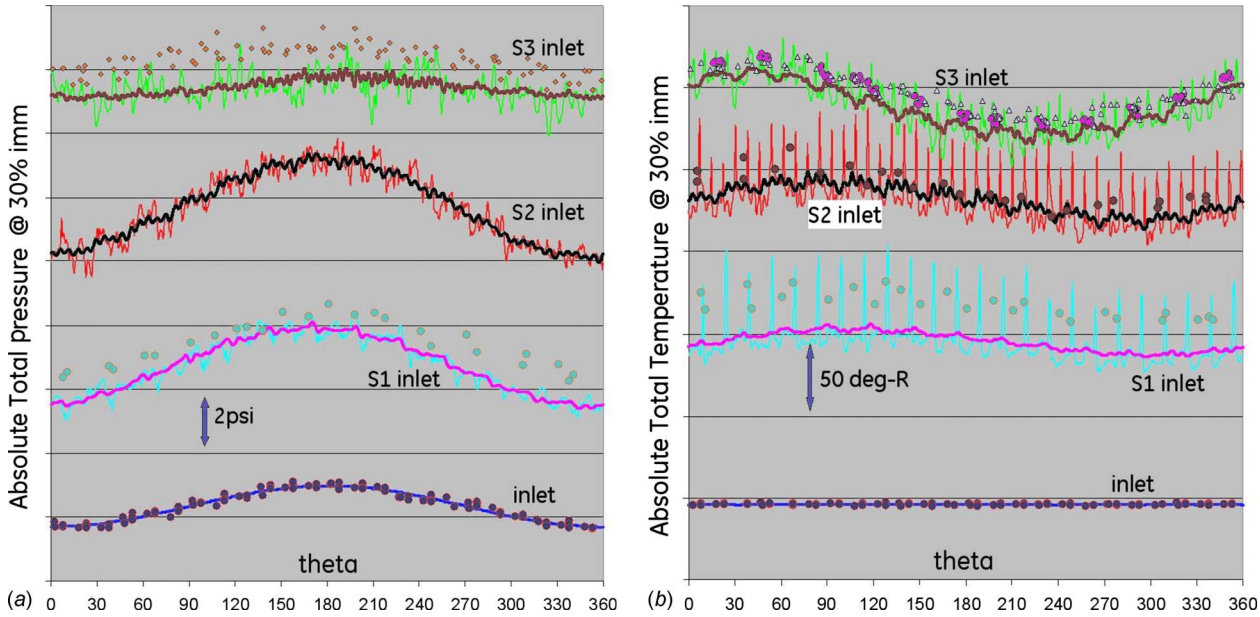

Fig. 6 Comparison of total pressure and total temperature profiles at about 30% immersion; first fan. Lines with rapid oscillation are the time instantaneous solution. Overlaid smoother lines are time-averaged solution. Solid symbols are measured data.

Downloaded 28 May 2010 to 128.113.26.88. Redistribution subject to ASME license or copyright; see http://www.asme.org/terms/Terms_Use.cfm

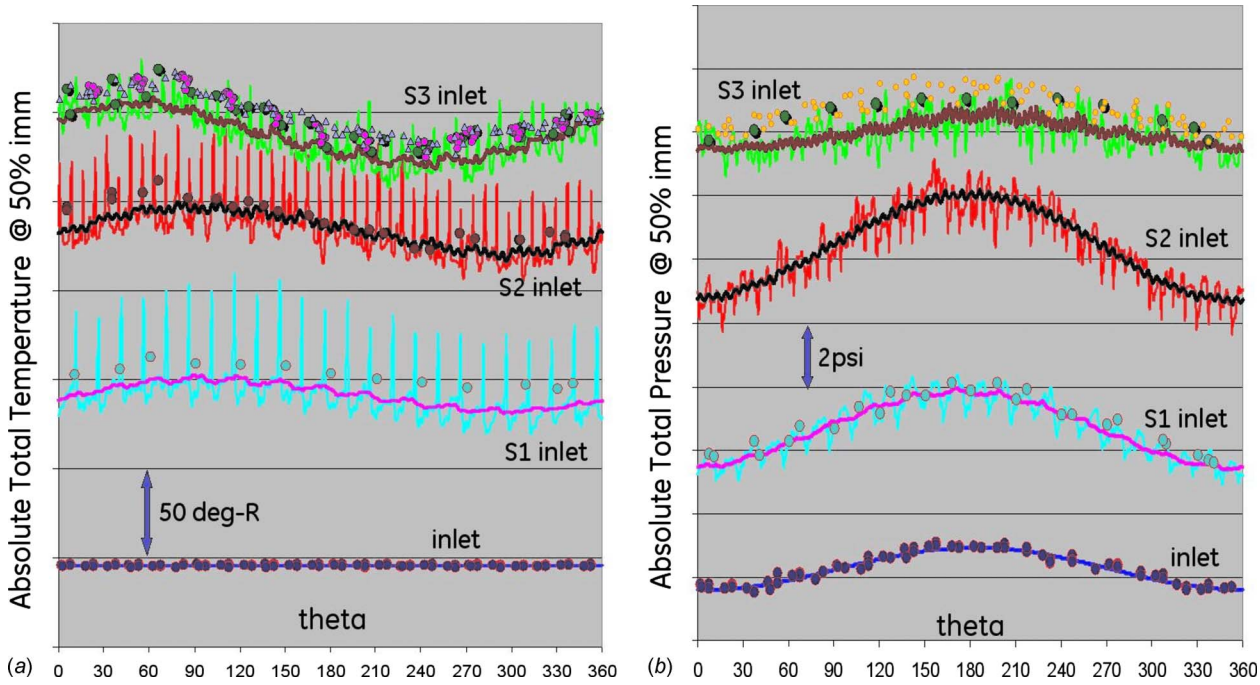

Fig. 7 Comparison of total pressure and total temperature profiles at about 50% immersion; first fan. Lines with rapid oscillation are the time instantaneous solution. Overlaid smoother lines are time-averaged solution. Solid symbols are measured data.

measured quantities were available at all immersions, and at certain immersions, only one probe had valid readings. At certain immersions and certain circumferential locations, the measurements showed scattering of data. This might be due to the fact that the distortion screen needed to be rotated to generate whole-wheel readings for a limited number of probes on the vanes. Two vanes per row were instrumented for this fan, and 13 distortion screen positions were used. It could also be an indication that certain sectors of the fan were more sensitive to upstream conditions than other sectors of the fan when distortion was present. This sensitivity will need further attention. The fan inlet total pressure and total temperature are also given in these plots as a reference.

Overall, the total pressure distortion transfer is predicted very well. No particular immersion had overwhelmingly better or worse comparisons. The total temperature distortion generation by Rotor-1 was predicted. The measurement showed that the total

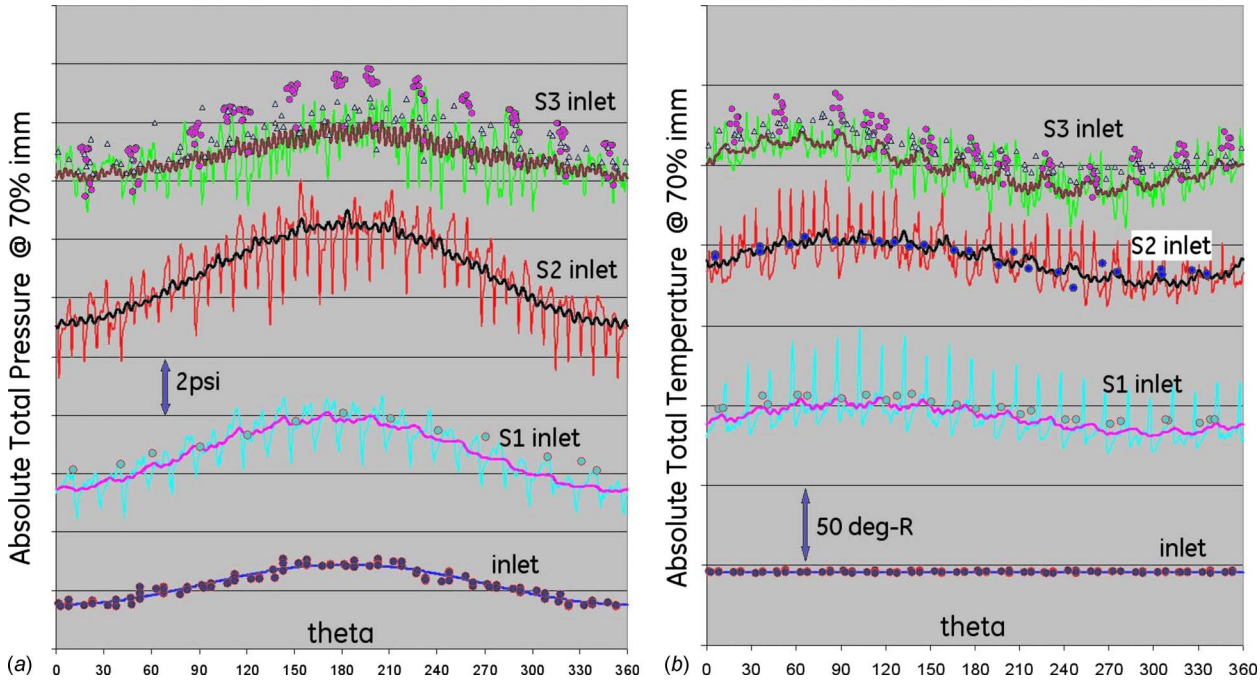

Fig. 8 Comparison of total pressure and total temperature profiles at about 70% immersion; first fan. Lines with rapid oscillation are the time instantaneous solution. Overlaid smoother lines are time-averaged solution. Solid symbols are measured data.

Downloaded 28 May 2010 to 128.113.26.88. Redistribution subject to ASME license or copyright; see http://www.asme.org/terms/Terms_Use.cfm

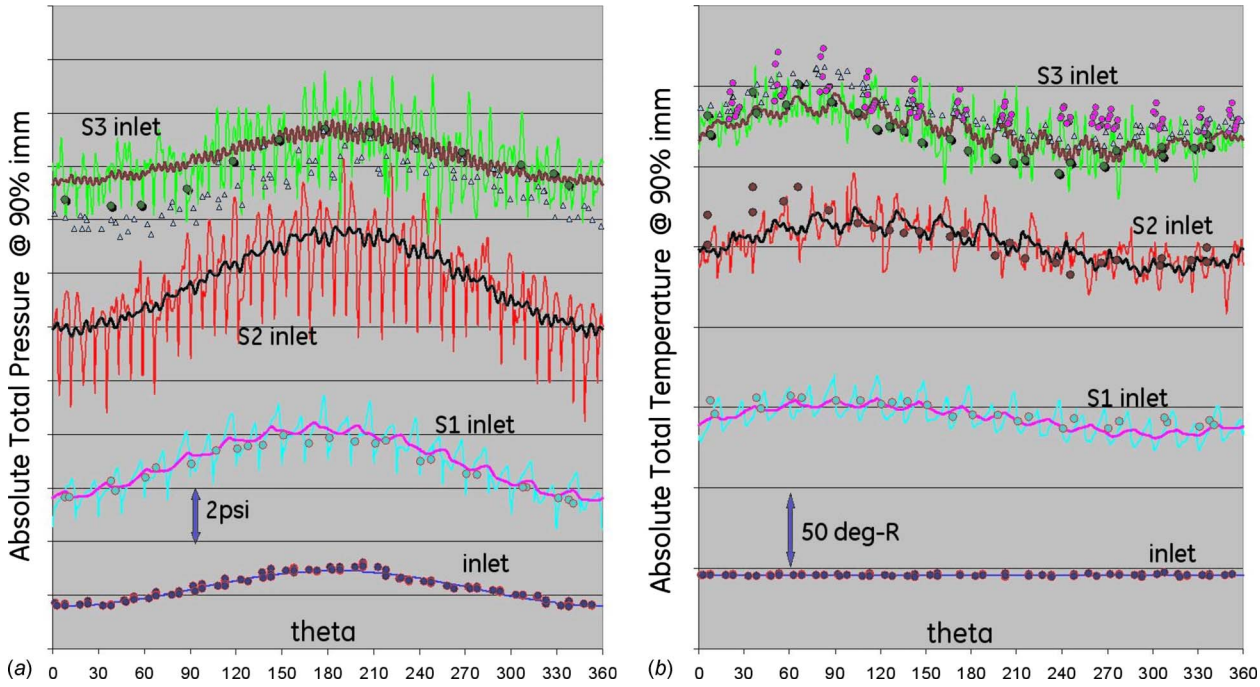

Fig. 9 Comparison of total pressure and total temperature profiles at about 90% immersion; first fan. Lines with rapid oscillation are the time instantaneous solution. Overlaid smoother lines are time-averaged solution. Solid symbols are measured data.

temperature profile (in circumferential direction) had a "phase lag" (about 90 deg in the direction of rotation) from the corresponding total pressure profile. This "phase" difference and its subsequent transfer to the downstream stages were accurately captured by the CFD simulations.

This fan was further throttled to a near-stall condition, where limited measurement was taken. This was due to the fact that only two stator vanes per row were instrumented with *Pt* and *Tt* probes, and the circumferential resolution was achieved via distortion screen rotation. The underlining assumption for this common setup is that the flow fields are the same (only differ in circumferential phase) for different screen positions. However, at the near-stall condition, this assumption is less valid than at normal operating conditions, hence only one screen position with which the data were taken. Figures 10–12 are the comparisons of total pressure and total temperature profiles at about 30%, 50%, and 70% immersions. The data match well to the numerical simulation results, thus providing confidence in the use of the simulation results to analyze the relevant flow physics.

3.2 Validation of the Second Multistage Fan. Similar to the first multistage fan, total pressure and total temperature measure-

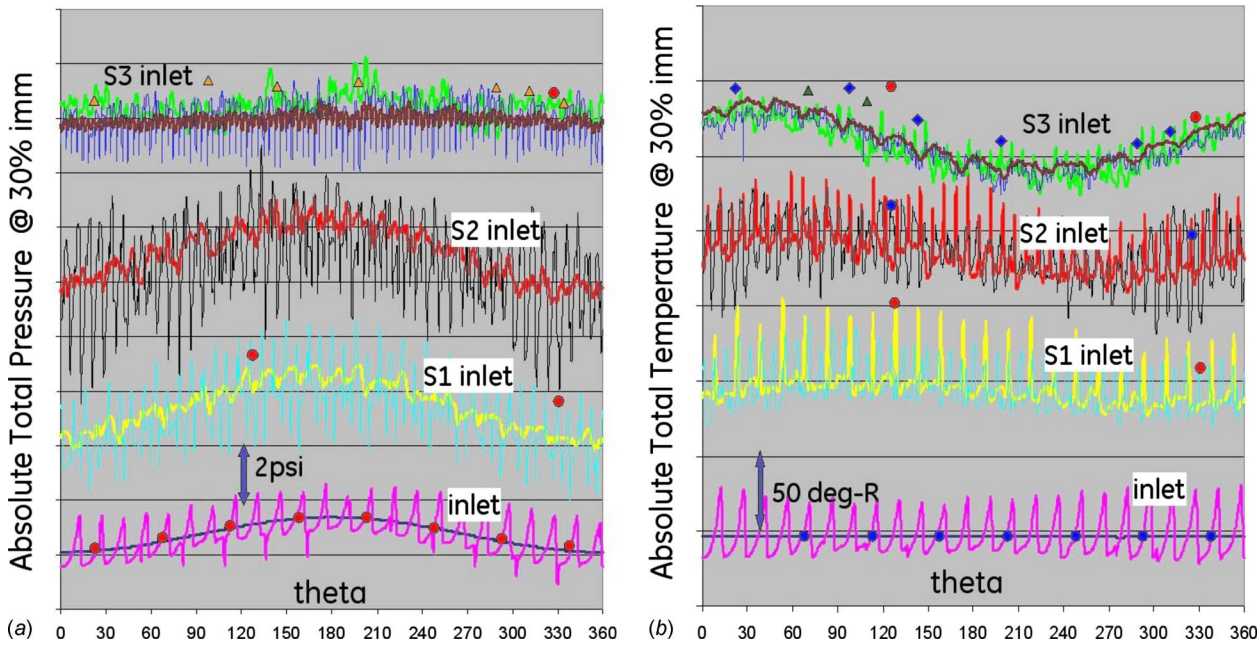

Fig. 10 Comparison of total pressure and total temperature profiles at about 30% immersion. First fan, near-stall condition.

Downloaded 28 May 2010 to 128.113.26.88. Redistribution subject to ASME license or copyright; see http://www.asme.org/terms/Terms_Use.cfm

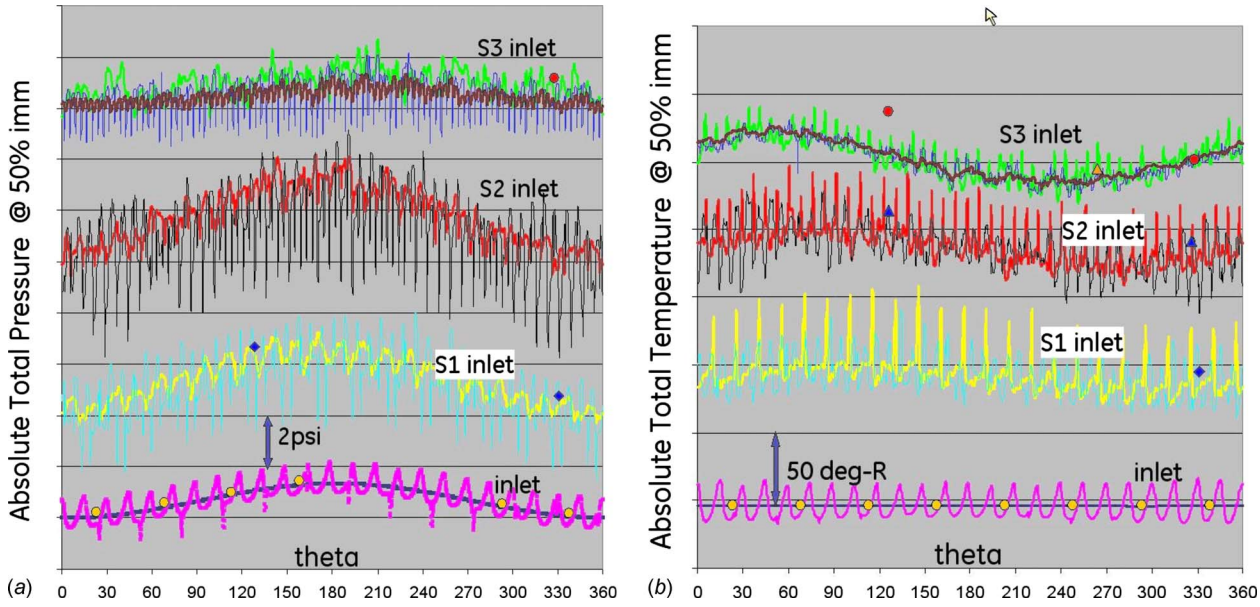

Fig. 11 Comparison of total pressure and total temperature profiles at about 50% immersion. First fan, near-stall condition.

ments were available at various radial locations at the leading edge of all three vanes. The fidelity of the measurement is about the same as that for the first fan for total pressure. Total temperature measurements at certain locations had less resolution than the first fan due to invalid readings from certain probes. Six vanes per stator row were instrumented, and three distortion screen rotations were used. Comparisons of the CFD results against data are included in this section for all available total pressure and total temperature data. The CFD results are time averaged from the time-accurate calculations covering one rotor revolution, which has 7350 physical time steps.

Figures 13–17 present comparisons of total pressure and total temperature at all five measured stator vane leading edge immersions. Comparisons are also presented at the fan exit. The plots for the fan exit are stacked on top of the main plots for clarity. There are less data scattering for this fan as compared with the data of the first fan. More total pressure and total temperature probes were installed; hence less rotation of the distortion screen was necessary to reach the same resolution as of the first fan. In general, the quality of experimental data was better for the second fan compared with the first fan. For the numerical simulations, however, there is no need to mimic the way the engine measurement was done. The computational domain includes all the blade passages of all the blade rows, with the inlet flow condition mapped to the entire inlet surface of the fan.

Overall, the total pressure distortion transfer was predicted very well. No particular immersion had overwhelmingly better or worse comparisons. Similar to the first fan, the total temperature distortion generation by Rotor-1 is evident and is matched by numerical simulation. The total temperature profile at Rotor-1 exit

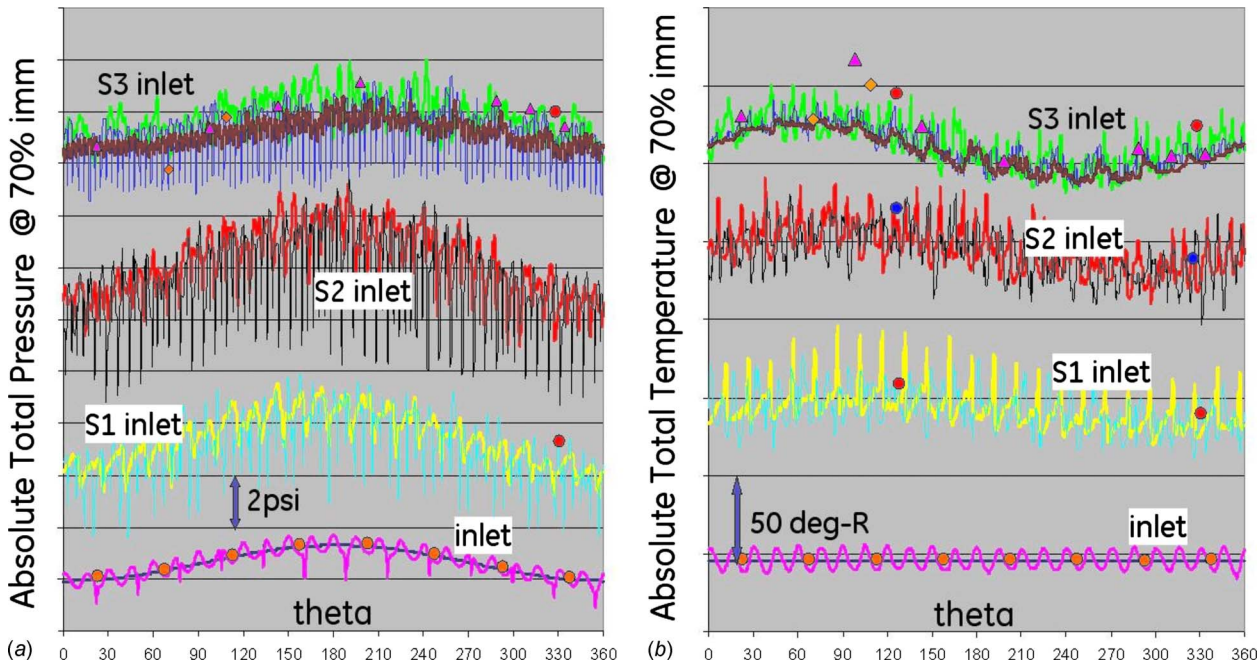

Fig. 12 Comparison of total pressure and total temperature profiles at about 70% immersion. First fan, near-stall condition.

Downloaded 28 May 2010 to 128.113.26.88. Redistribution subject to ASME license or copyright; see http://www.asme.org/terms/Terms_Use.cfm

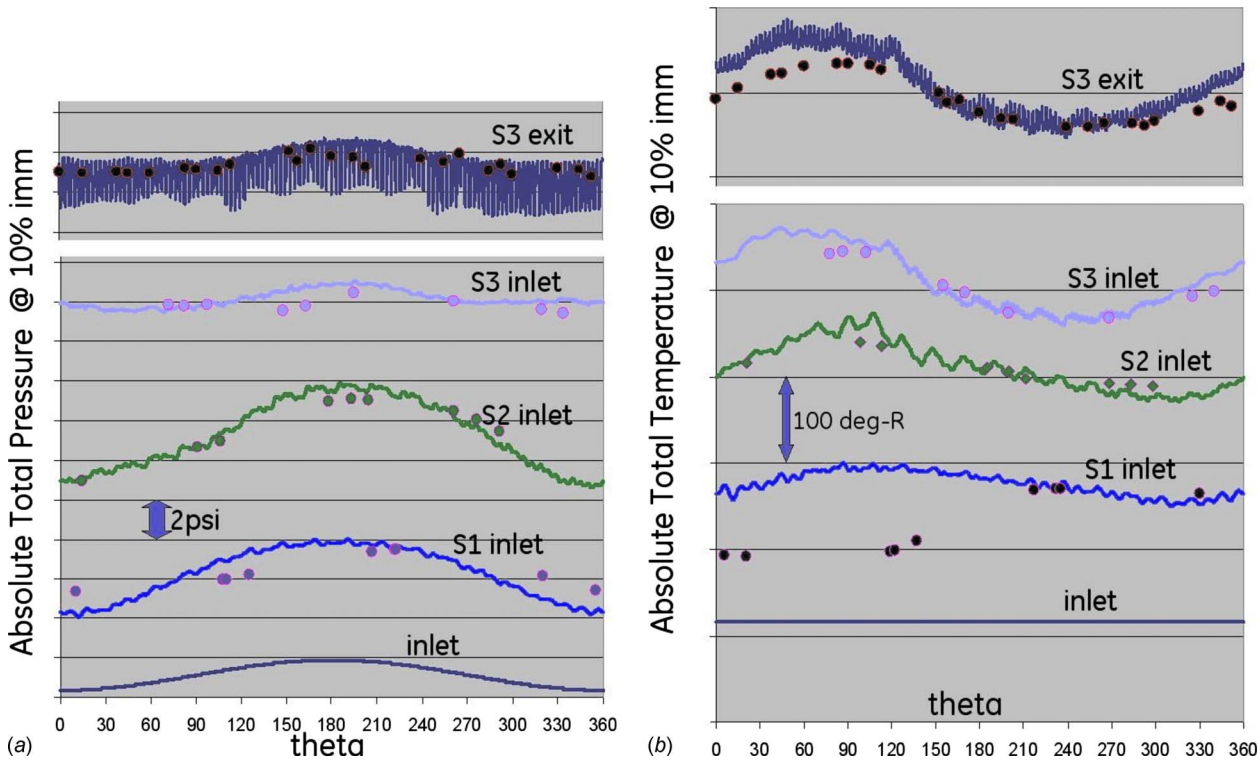

Fig. 13 Comparison of total pressure and total temperature profiles at about 10% immersion; second fan. Lines with rapid oscillation are the time instantaneous solution. Overlaid smoother lines are time-averaged solution. Solid symbols are measured data.

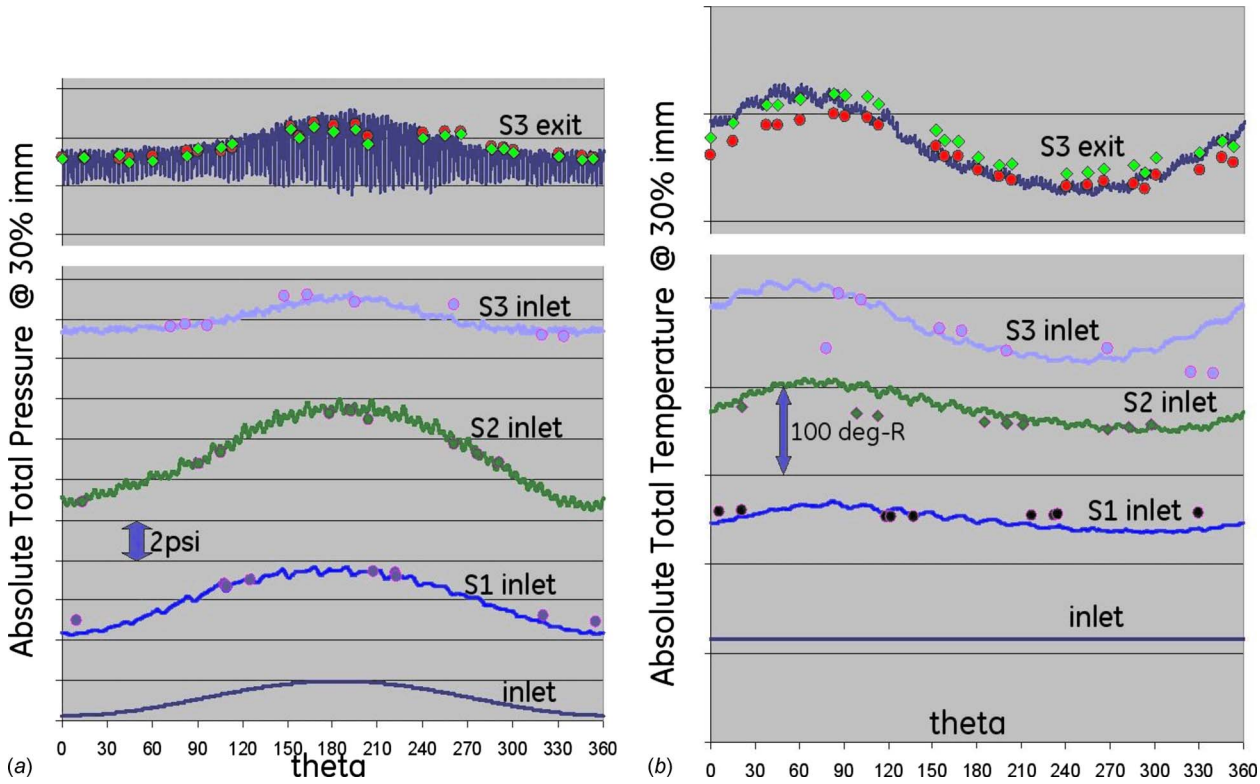

Fig. 14 Comparison of total pressure and total temperature profiles at about 30% immersion; second fan. Lines with rapid oscillation are the time instantaneous solution. Overlaid smoother lines are time-averaged solution. Solid symbols are measured data.

Downloaded 28 May 2010 to 128.113.26.88. Redistribution subject to ASME license or copyright; see http://www.asme.org/terms/Terms_Use.cfm

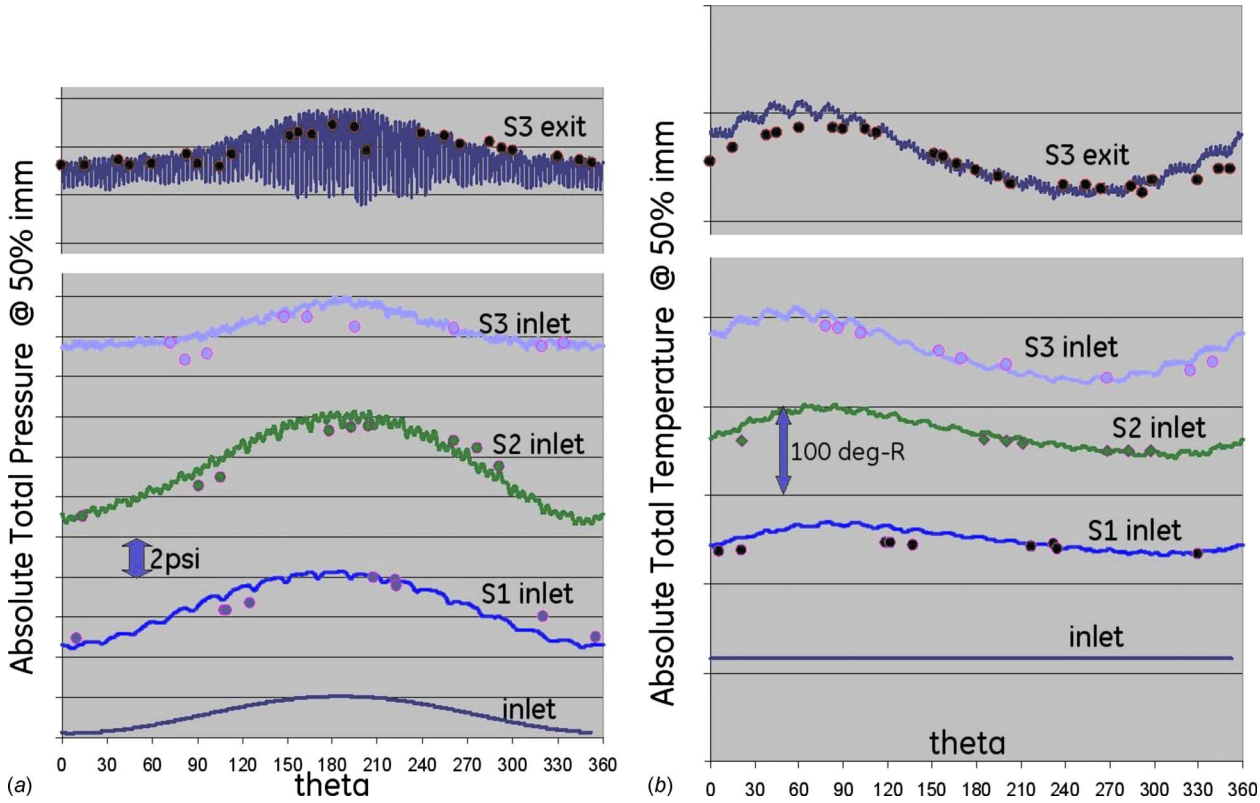

Fig. 15 Comparison of total pressure and total temperature profiles at about 50% immersion; second fan. Lines with rapid oscillation are the time instantaneous solution. Overlaid smoother lines are time-averaged solution. Solid symbols are measured data.

exhibits a 90 deg "phase lag" from the total pressure profile. The generation and subsequent transfer of the total temperature distortion, as well as the total pressure distortion propagation, were closely matched by the numerical simulation.

The validation for both multistage fans is considered excellent, establishing confidence in high-fidelity CFD capability to predict distortion transfer and, in general, the overall work output of each fan stage. The validation is significant for the following reasons. First, it establishes the foundation for both higher-fidelity integrated inlet/fan simulations and lower-fidelity reduced-order modeling of distortion transfer. Second, it shows the value of bringing unsteady CFD into earlier stages of the engine design process to assess distortion handling capability before the hardware is built. A consequence is more accurate predictions of pressure and temperature profiles entering the core compressor. It can also be used as a virtual test tool to study distortion management schemes. It can guide engine distortion characterization to achieve better test methodology and to reduce the number of tests that need to be performed. Third, the validation is not tied to one particular CFD flow solver; it is essentially an assessment of the general capability of unsteady RANS. The CFD requirement can be met by any well-written CFD flow solver of compressible unsteady RANS.

4 Spatial Phase of Total Pressure and Total Temperature Profiles

A notable feature observed in both data and CFD results was that the total temperature profile had about 90 deg phase difference in the circumferential direction. Compared to the high peak of the total pressure profiles, the high peak of the total temperature profiles lags behind by about 90 deg. The total pressure high peak is leading in the direction of rotation. For the distortion propagation, the total pressure profiles largely stays in phase as it progresses through the fan (small phase shifts are observed), and the total temperature distortion profiles, with a large phase difference by the first stage, progresses through the fan with rather small shifts (further lags) by the second and the last stage.

This observation was introduced in Part I of this paper by the authors [1]. That discussion was from the equation-of-state perspective, which highlighted the role of density variation. The density role is often neglected by distortion transfer models, which assume incompressible flow. Part I suggested that the spatial phase of the stagnation parameters was dictated by the respective static parameters. With the complete fan domain modeled in this paper, this concept is re-examined to better understand the mechanism. Figure 18 shows the static pressure and static temperature profiles throughout the first fan. The purpose of examining the static parameters is to comprehend the role of velocity distortion since the stagnation parameters have an overall "masquerading" effect and may not reveal the underlying mechanism completely. There are two major findings. First, the static pressure profile shifts every time it passes through a blade row, either a rotor or a stator row. The total pressure profiles, however, do not show this "zigzag" shifting pattern. Second, the static temperature profiles closely mimic the total temperature profiles, suggesting that the static temperature profile is dominating the total temperature phase. This leaves the velocity distortion to a nonimportant role in terms of phasing. It is worth noting that the profiles of these parameters are not in strict sinusoidal form anymore. In the positive pressure gradient sector (0–180 deg), it has a fuller (convex) shape than a sinusoidal form, while at the negative pressure gradient sector (180–360 deg), it has a more concaved form than a sinusoidal function. On the other hand, it is important to point out that the density has distortion as well (see Fig. 19). The velocity profile has its own propagation behavior, with the largest distortion at IGV inlet and much less distortion level at all stator inlets.

Mazzawy [2] attributed the total temperature phase difference to angular particle displacement, and was able to incorporate the

Downloaded 28 May 2010 to 128.113.26.88. Redistribution subject to ASME license or copyright; see http://www.asme.org/terms/Terms_Use.cfm

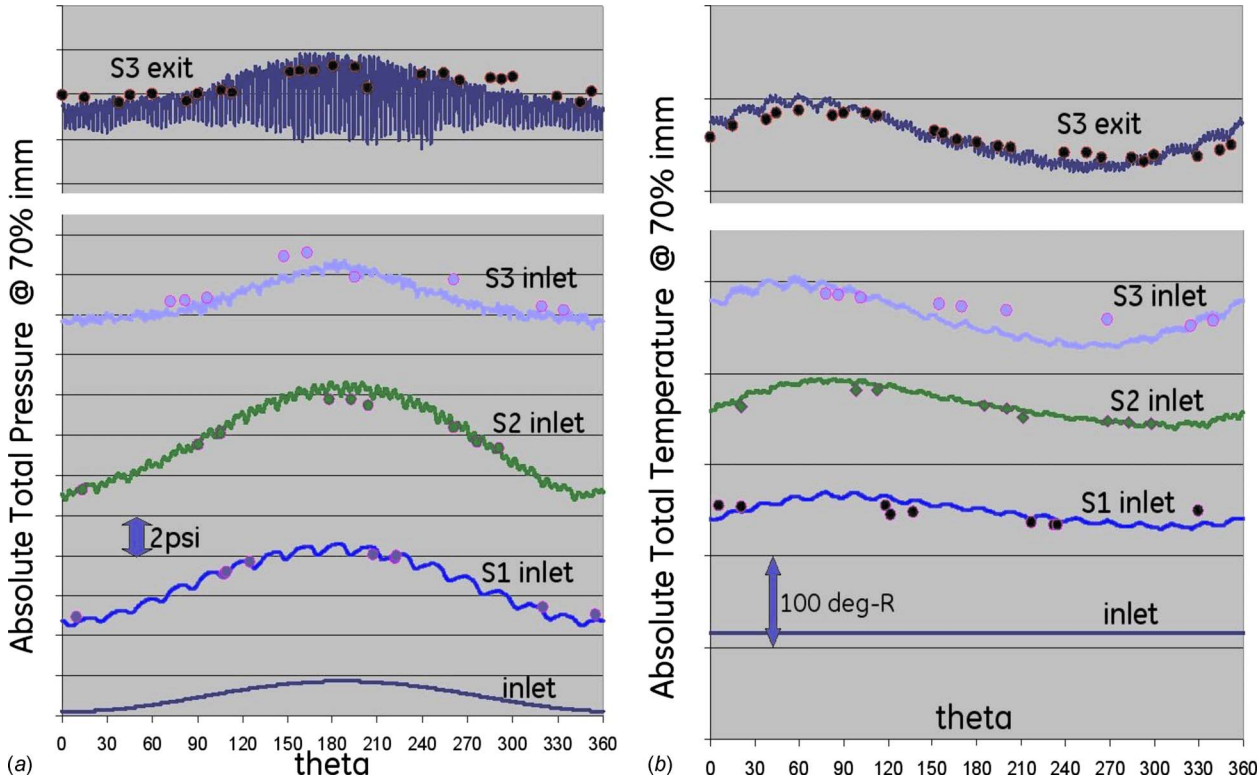

Fig. 16 Comparison of total pressure and total temperature profiles at about 70% immersion; second fan. Lines with rapid oscillation are the time instantaneous solution. Overlaid smoother lines are time-averaged solution. Solid symbols are measured data.

particle displacement in a multisegment parallel compressor model to match data significantly better. From the Lagrangian perspective, while the fluid particles are transported by the rotor blades, the properties of the particles (i.e., pressure and temperature) are altered as they pass though the blade passage. A particle at rotor inlet with the highest temperature of the incoming flow may not be at the high peak of the temperature profile downstream of the rotor at the displaced circumferential location. With a uniform Rotor-1 inlet total temperature, the particle displacement analogy does not explain the total temperature distortion generation by Rotor-1 with a 90 deg phase difference. Using the average axial velocity component at the midspan in the low *PTA* (low axial velocity) section, the estimated particle displacement using $\Delta\theta=(b/u)\omega$ is 52 deg (positive in the direction of rotation), where b is the axial chord length, u is the axial velocity, and ω is the angular wheel speed. This angle is then offset by the Rotor-1 blade stagger angle, and the net angular displacement is about 9 deg ahead of the particle location at the Rotor-1 inlet. This does not agree with total pressure and total temperature profiles from either data or CFD results (total pressure high peak is leading the total temperature high peak in the direction of rotation), although the particle angular displacement certainly exists in the flow.

It is important to note that the apparent phase shift is *not* a literal shift. It is the result of pressure and temperature rise caused by the blade rows operating at inlet and discharge conditions that vary in the circumferential direction. To uncover the mechanism, both the static pressure and static temperature rise of each stage are examined and shown in Figs. 20 and 21 for both multistage fans. In each of the figures, there are three individual plots that are stacked up for the clarity to show the profiles for each stage. Static pressure rise is normalized by density and C_p to arrive at the same level of static temperature rise. These two figures, showing the pressure and temperature rise of both fans, clearly illustrate the correlation between the pressure rise and the temperature rise. The temperature rise through Rotor-1 is directly related to the pressure rise of the same rotor, this in turn leads to the generation of the observed total temperature distortion generation by Rotor-1 (velocity profile at Rotor-1 exit is relatively flat, see Fig. 19), and explains the phase difference of the resultant total temperature profile. Note that the Rotor-1 inlet static temperature profile is affected by the local velocity distortion due to the uniform total temperature profile at fan inlet. This finding is also explained by Gibb's equation, $Tds=dh-dp/\rho$. The entropy change in this equation may include flow state change between inlet and exit among other factors.

Figures 20 and 21 reveal that pressure and temperature distortions are generated and transferred quite differently by each individual stage. Across the first stage, the peak pressure rise is not at the same location of the high peak of the incoming pressure profile, rather it lags quite a distance from the high peak of the incoming pressure profile. Combined with the incoming temperature (which is influenced by the velocity distortion since the inlet total temperature is constant), the temperature profile high peak rests at about 90 deg in the fan circumference. Similar explanation can be found for the low peak of the temperature profile. The second stage, however, has a relatively flat pressure rise profile. It shifts whatever the incoming profile of pressure to a higher level by applying relatively uniform pressure rise. There are other factors, i.e., inlet swirl distortion, that might drive small changes in the pressure and temperature profiles for the middle stage. The distortion level at the second stage (discussed in Sec. 5) may appear to be lower because of the increased overall pressure level at the second stage, but the amount of distortion remains largely unchanged. The last stage (Rotor-3) has a pressure rise profile almost in the mirror image of the incoming pressure profile. This is due to the Rotor-3 discharge pressure profile that is relatively flat. Rotor-3 is thus "forced" to attenuate the distortion, which has been amplified by the upstream stages. The relatively flat discharge pressure profile is determined due to large axial space in-between the fan exit and the splitter of bypass and core. As a

Downloaded 28 May 2010 to 128.113.26.88. Redistribution subject to ASME license or copyright; see http://www.asme.org/terms/Terms_Use.cfm

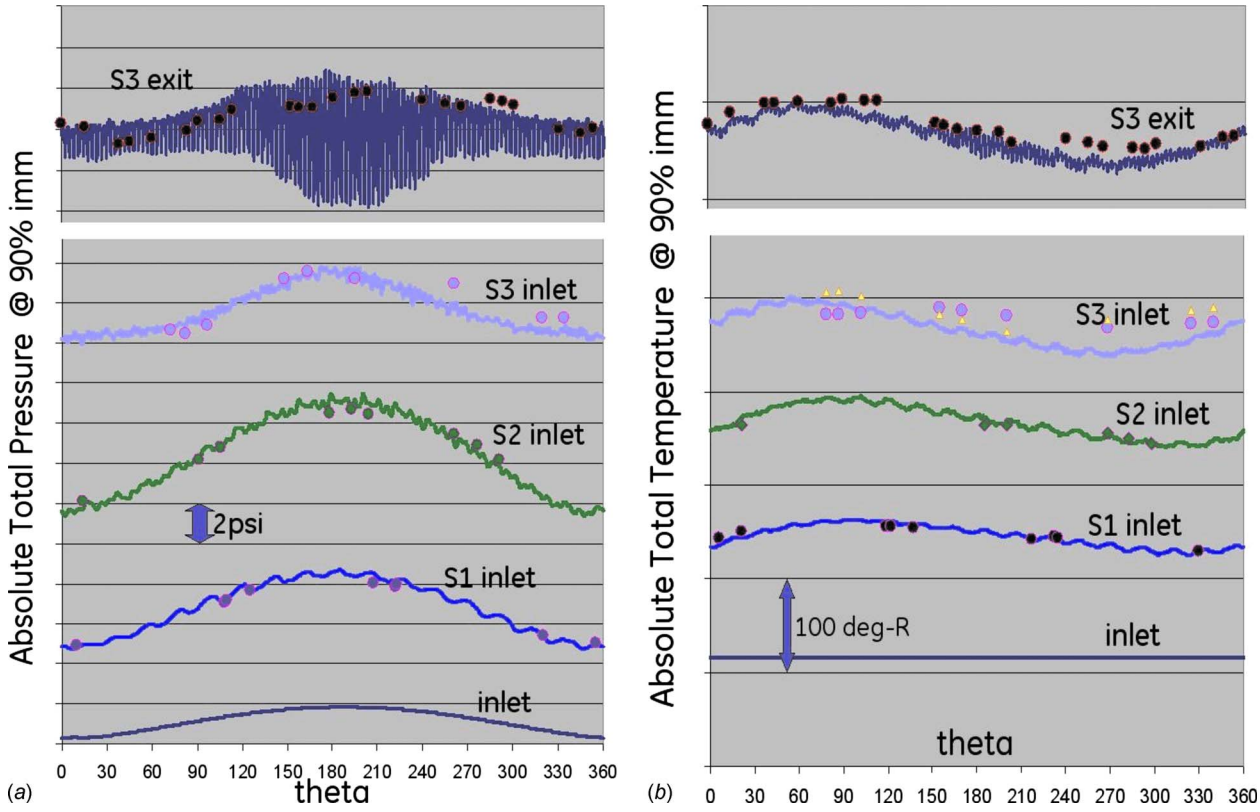

Fig. 17 Comparison of total pressure and total temperature profiles at about 90% immersion; second fan. Lines with rapid oscillation are the time instantaneous solution. Overlaid smoother lines are time-averaged solution. Solid symbols are measured data.

result, Rotor-3 passages are effectively throttled as they pass through the pressure distortion at inlet. The stability margin of Rotor-3 is therefore consumed even though the overall engine throttle remains constant. This stage (rotor) is more likely to be the limiting stage in the multistage environment, and needs to have plenty room in the stall margin by design.

It needs to be noted that the total pressure and total temperature phase difference is not a universal phenomenon, as it can be seen from the above analysis. Among some other GE fans, the phase difference varies significantly. The dominating factors and their roles for the *PTA*/*TTA* phase difference remain as a research topic. Furthermore, whether and how this phase difference affects the stability margin is a question that needs to be answered.

5 Distortion Transfer and Generation

Detailed discussion is presented in this section for total pressure distortion transfer, the generation of total temperature distortion,

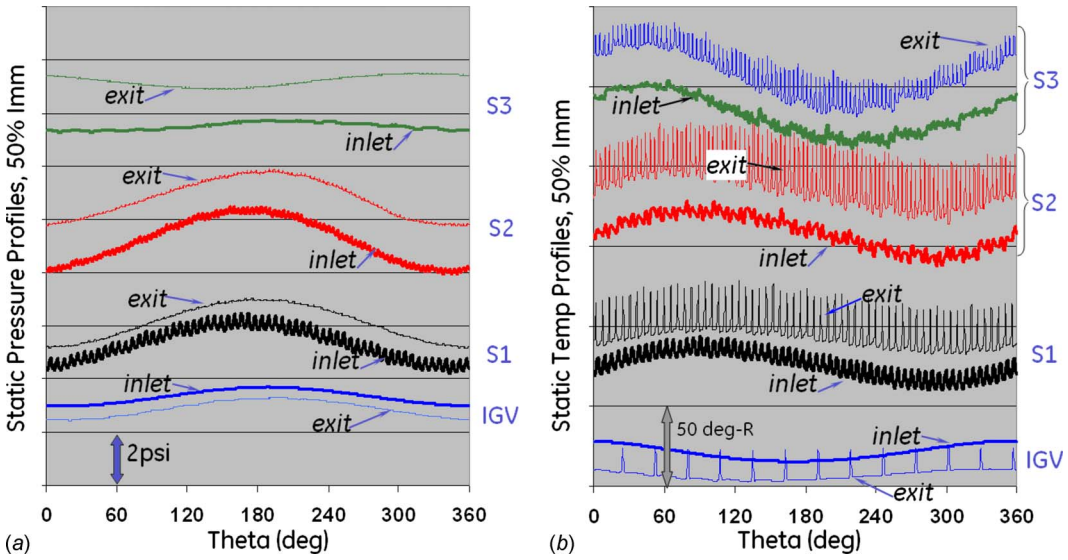

Fig. 18 Static pressure and static temperature profiles of the first fan at about 50% immersion

Downloaded 28 May 2010 to 128.113.26.88. Redistribution subject to ASME license or copyright; see http://www.asme.org/terms/Terms_Use.cfm

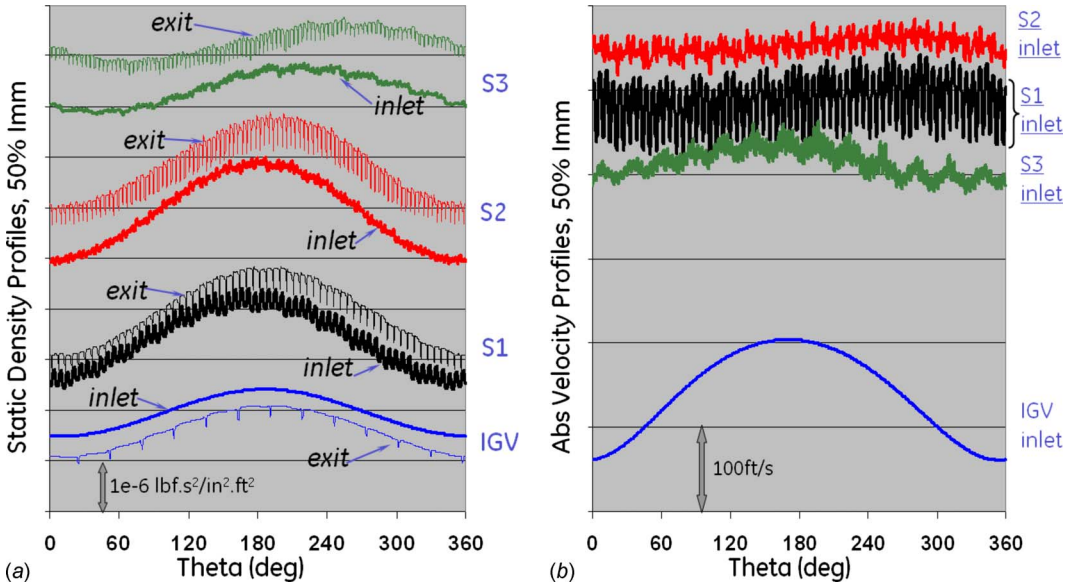

Fig. 19 Density and absolute velocity profiles of the first fan at about 50% immersion

and the swirl distortion. The distortion levels for both fans are plotted using the same scale for comparison purposes. The transfer of the total pressure distortion can be initially observed from the validation section above. To highlight the distortion transfer, the ARP-1420 standard was used for defining distortion levels and was applied to various immersions of the fan to examine the transfer behavior. The definitions are recited as follows:

$$PT\_\text{distortion level}_{\text{local}} = PTDL_{\text{local}} = \frac{PT_{\text{avg}} - PT_{\text{min}}}{PT_{\text{avg}}}$$

$$TT\_\text{distortion level}_{\text{local}} = TTDL_{\text{local}} = \frac{TT_{\text{max}} - TT_{\text{avg}}}{TT_{\text{avg}}}$$

5.1 First Multistage Fan. The stage-by-stage distortion level at various immersions is shown in Figs. 22–24. In those plots, distortion levels for both the stagnation and static parameters are included. For total pressure distortion, at all the immersions, the inlet distortion is amplified by the first stage and is then slightly attenuated by the second stage. The distortion level by the second

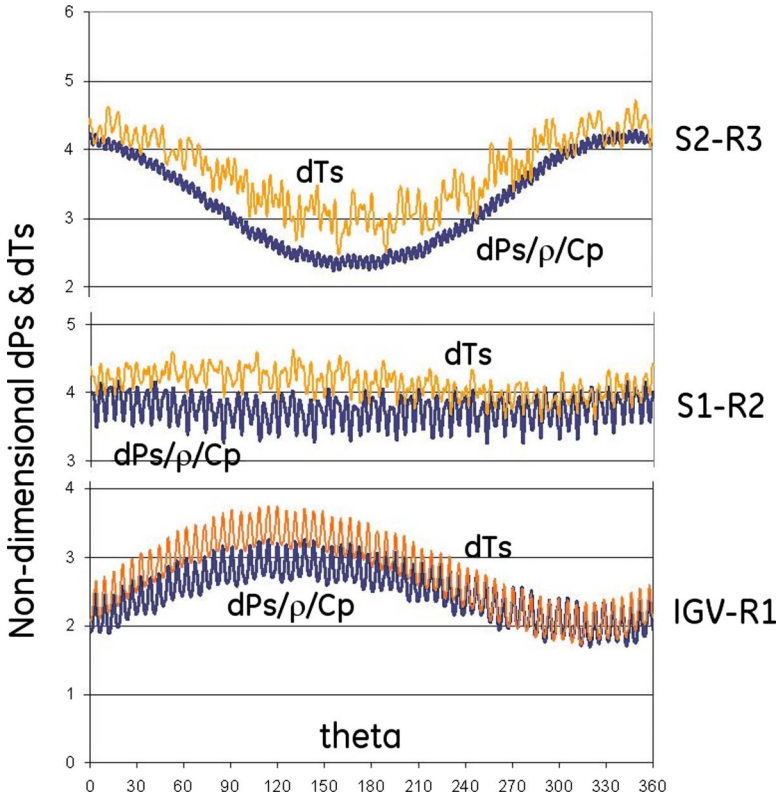

Fig. 20 Static pressure and static temperature rise across the first fan at 50% immersion

Downloaded 28 May 2010 to 128.113.26.88. Redistribution subject to ASME license or copyright; see http://www.asme.org/terms/Terms_Use.cfm

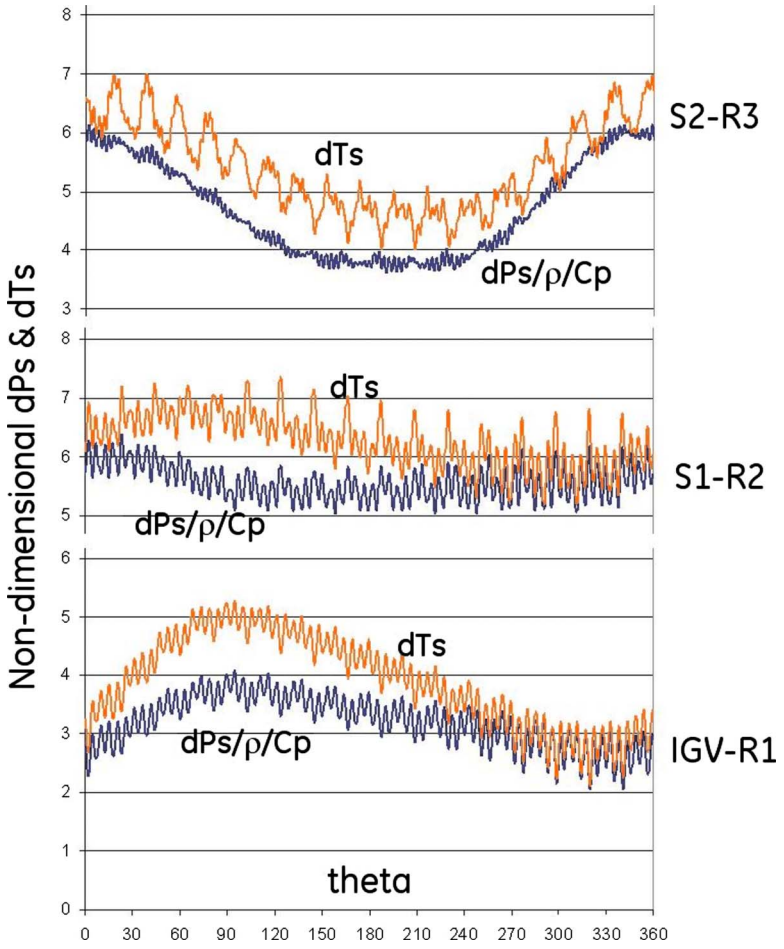

Fig. 21 Static pressure and static temperature rise across the second fan at 50% immersion

stage is still significantly higher than the inlet distortion level. This elevated distortion level is significantly attenuated by the last stage, for all the immersions, though the tip section shows more attenuation than at the hub section. More attenuation at the tip section is due to steeper characteristics at the tip than at the hub section.

Total temperature distortion is generated when the flow passes through the first stage. As the flow progresses downstream, more distortion is generated. At 50% immersion, the total temperature distortion level exhibits a linear trend of growth. The significant

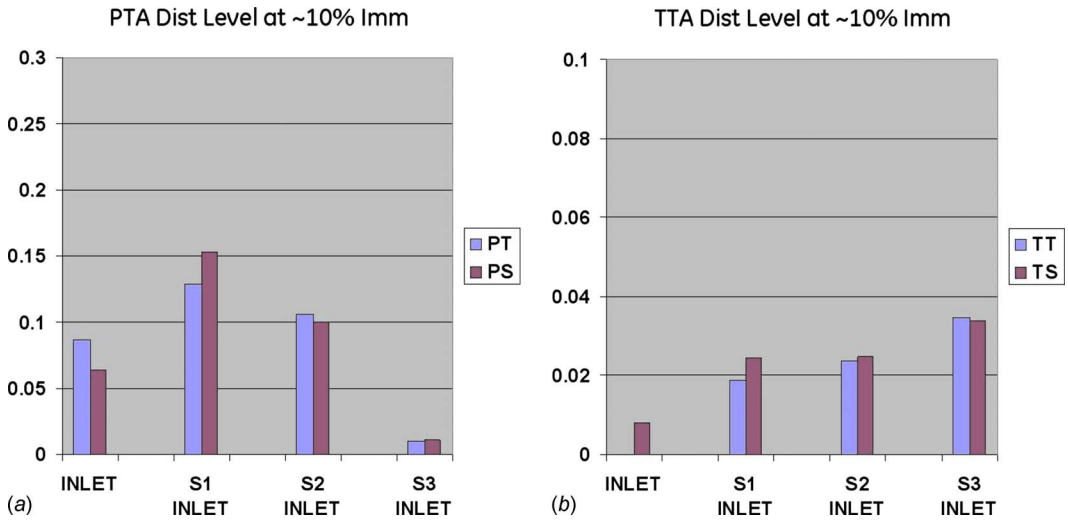

Fig. 22 Comparison of total pressure and total temperature distortion levels at about 10% immersion; first fan

Downloaded 28 May 2010 to 128.113.26.88. Redistribution subject to ASME license or copyright; see http://www.asme.org/terms/Terms_Use.cfm

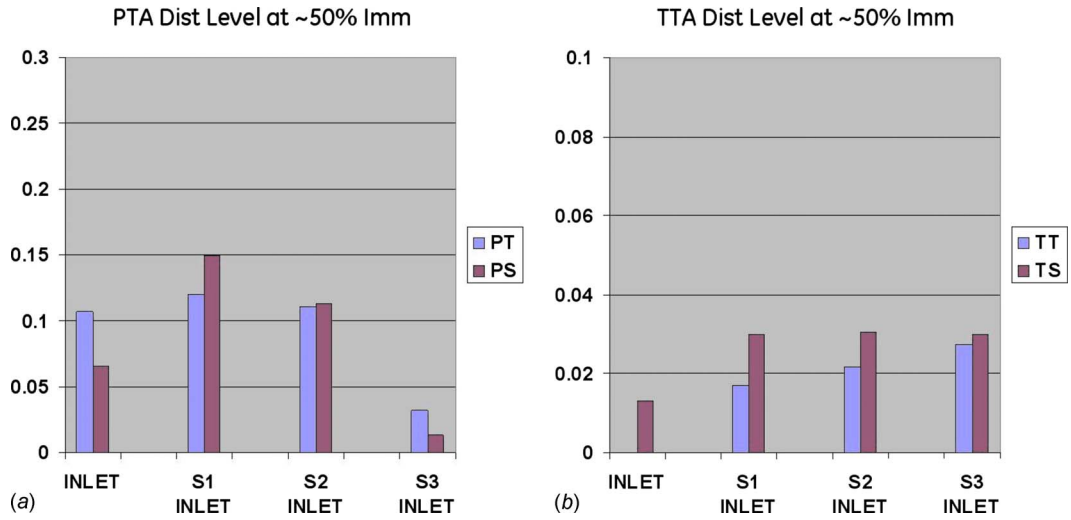

Fig. 23 Comparison of total pressure and total temperature distortion levels at about 50% immersion; first fan

attenuation of the total pressure distortion by the last (third) stage does not seem to cause the generation of total temperature distortion to be above the linear trend. However, this is not the case near the tip section. At 10% immersion, the total temperature distortion level at the last stage does seem to respond to the rapid attenuation of total pressure distortion by the last stage. A surprise comes from the hub section at about 90% immersion, where there is a similarly rapid attenuation of the total pressure distortion by the last stage but to a lesser degree as compared with the other immersions. From the first stage to the second, the total temperature distortion responds with a 50% increase (in distortion level) to a mild total pressure distortion attenuation by the middle (second) stage. However, from the second stage to the third, the temperature distortion level decreases in response to a rather significant attenuation of pressure distortion by the third stage. This reveals the nonlinear nature of distortion generation and transfer, and a certain degree of separation of correlation between the total pressure distortion and total temperature distortion. The common belief that more *PTA* distortion attenuation leads to more *TTA* distortion generation is thus conditionally true. Examining the stage/blading design philosophy together with the CFD results could lead to designs with low pressure distortion transfer (more attenuation) and low temperature distortion generation.

The static pressure distortion largely follows the trend of the total pressure distortion. The most significant amplification is seen by the first stage, where the static pressure distortion level is more than doubled from the inlet. This comes with the fact that the total pressure ratio of the first stage is the highest among the three stages, whereas the static pressure rise across the first stage is the least among the three stages.

5.2 Second Multistage Fan. The stage-by-stage distortion level at various immersions is shown in Figs. 25–27. Distortion levels for both the stagnation and static parameters are included in these plots. Compared to the first fan, the following observations can be made.

1. The inlet distortion level is significantly higher than that of the first fan; as a result, the distortion levels at each stage are significantly higher.
2. The general behavior of the distortion transfer is similar to that of the first fan. However, some differences are observed. At 10% immersion, the total pressure distortion level at Stator-2 inlet is about the same as the distortion level at the

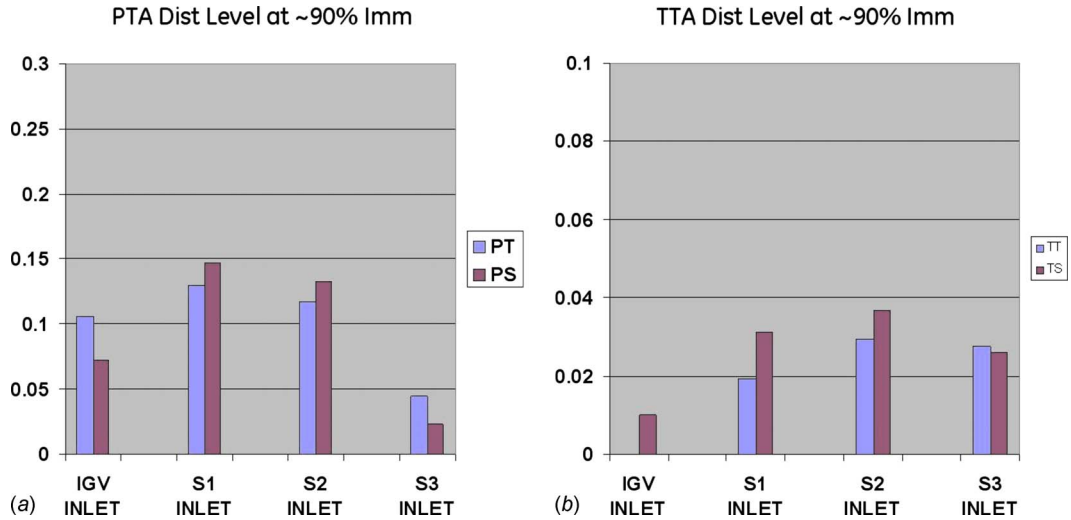

Fig. 24 Comparison of total pressure and total temperature distortion levels at about 90% immersion; first fan

Downloaded 28 May 2010 to 128.113.26.88. Redistribution subject to ASME license or copyright; see http://www.asme.org/terms/Terms_Use.cfm

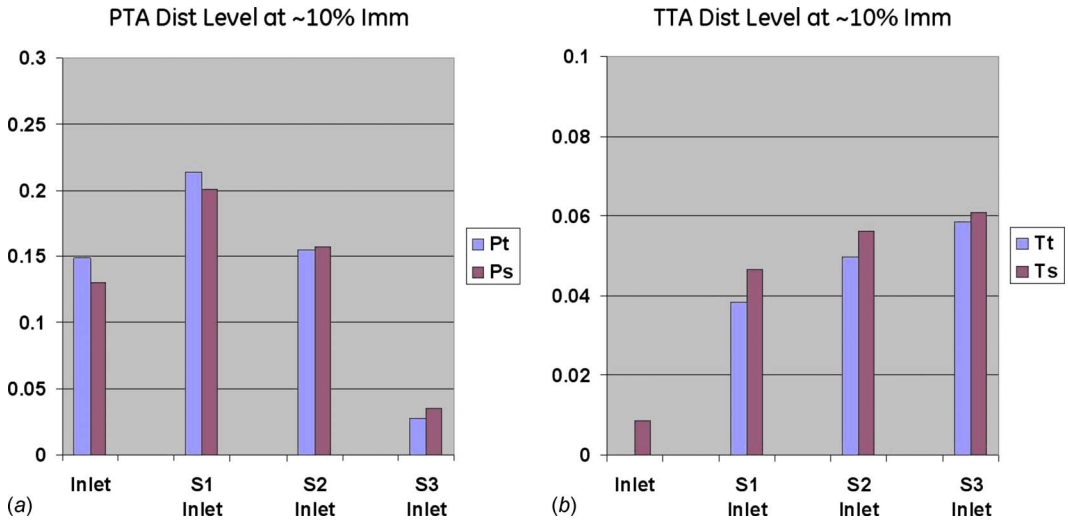

Fig. 25 Comparison of total pressure and total temperature distortion levels at about 10% immersion; second fan

fan inlet, while for the first fan, the distortion level at Stator-2 inlet is still higher. This is true for other immersions as well, that the total pressure distortion level at Stator-2 inlet is at or below the distortion level at the fan inlet. This could be due to the higher overall pressure level at Stator-2 inlet generated by a higher pressure ratio of the Rotor-2.

3. For total temperature distortion levels, at 10% immersion, no growth is found above the linear trend by the last stage as is it true for the first fan. At 90% immersion, the total temperature distortion level does not dip below the distortion level at the Stator-2, as it is the case for the first fan.

These differences in distortion transfer do not really underscore a significant change in transfer behavior, even though the two fans were designed with quite different philosophies.

5.3 Generation of Swirl Distortion. Due to the fan response to the inlet pressure distortion, not only the total temperature distortion is generated, but also swirl distortions are generated as well. Figure 28 presents the absolute swirl profiles of the first fan at stator leading edges with special attention to the IGV. The second fan has very similar swirl distortion profiles. There are two different kinds of swirl distortions being observed from the numerical simulations of the two multistage fans. The first kind is the induced swirl upstream to the fan inlet. This is due to the imbalance of the static pressure in the circumference caused by the total pressure distortion. This imbalance of the static pressure gives rise to a secondary flow that goes from high pressure sector to low pressure sector. Near the leading edge of the IGV, the induced swirl distortion reaches ± 10 deg. The IGV removes this induced swirl distortion significantly, illustrating the important role of the IGV. The remnant induced swirl distortion is absorbed by the Rotor-1. Details of the swirl distortion were reported by the authors in 2007 [3]. The other kind of swirl distortion is generated by the rotor blades in response to the distorted inflow, be it total pressure distortion alone or combined total pressure and total temperature distortions. This kind of swirl distortion can be observed downstream of Rotor-1 and all the way across the fan. It has different spatial phase than the induced swirl at the fan inlet. Significant amount of swirl distortion is generated by the last stage rotor, which is "forced" to attenuate the elevated total pressure

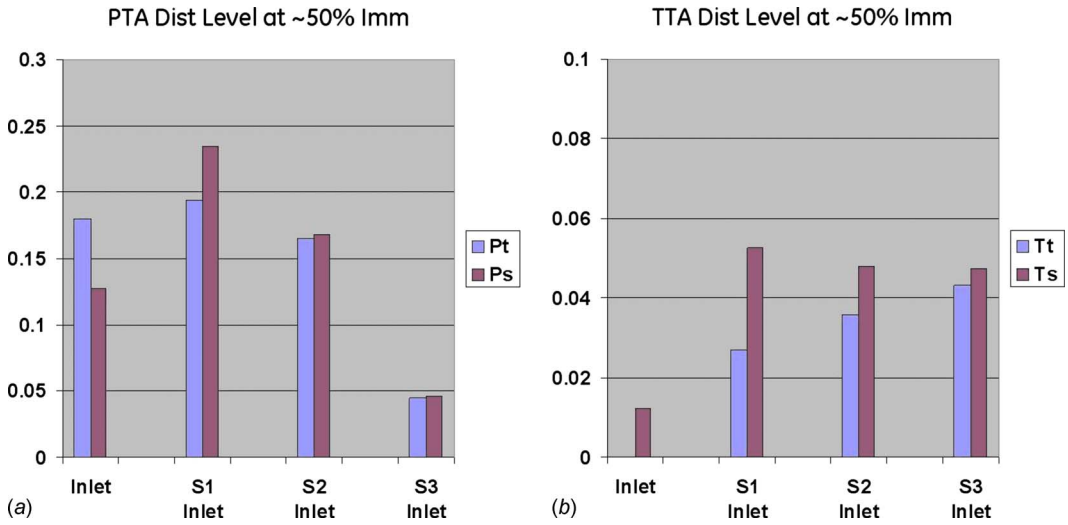

Fig. 26 Comparison of total pressure and total temperature distortion levels at about 50% immersion; second fan

Downloaded 28 May 2010 to 128.113.26.88. Redistribution subject to ASME license or copyright; see http://www.asme.org/terms/Terms_Use.cfm

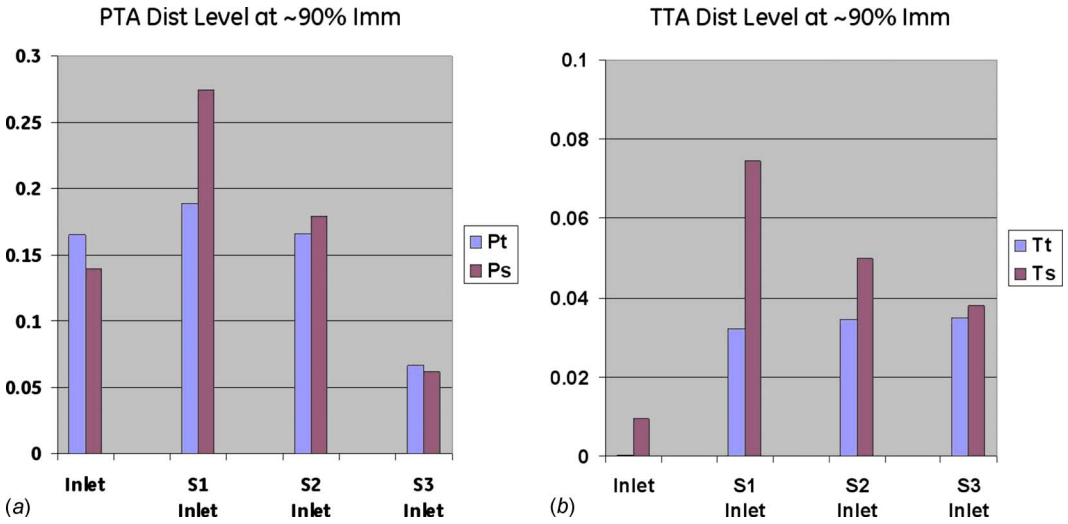

Fig. 27 Comparison of total pressure and total temperature distortion levels at about 90% immersion; second fan

distortion at Rotor-3 inlet. The swirl distortion by the last stage rotor is effectively removed by the fan OGV (Stator-3, not shown).

6 Conclusions

Unsteady RANS calculations were successfully applied to predict the 1/rev inlet total pressure distortion transfer in the entirety of two differently designed multistage fans. This is a significant advance from the numerical experiments reported in the Part I of this paper. The following conclusions were drawn from the analysis of the numerical results and the comparisons of CFD to engine test data.

1. High-fidelity CFD is further demonstrated to be able to predict the distortion transfer accurately for multistage fans. The work split among the stages is accurately predicted as well. This demonstration validates and verifies the general capability of the unsteady RANS flow solvers. It lays a foundation for higher-fidelity integrated inlet/fan simulations and serves as a resource for reduced-order modeling. high-fidelity CFD can be brought in early design process for verification purposes before hardware is built and can be used to guide the distortion characterization in distortion tests, hence reducing engine development cost.
2. Even with inlet total pressure distortion alone, both fans see the distortion of total temperature and swirl, generated in the multistage environment. Therefore, this validation is not just for the inlet total pressure distortion but also for three major distortion types.
3. Detailed analysis of the CFD results has led to a thorough understanding of the total temperature distortion generation and transfer mechanism, especially for the spatial phase difference of total pressure and total temperature profiles. This illustrates that the static parameters are more revealing than their stagnation counterpart and that pressure and temperature rise are more revealing while the pressure and temperature ratio could be misleading.
4. The total pressure distortion transfer behavior is analyzed at various immersions and in a stage-by-stage fashion. The first stage amplifies the inlet distortion, while the second stage carries it along. The distortion level to the last stage is either at or higher than the distortion level at the fan inlet. The last stage, subjecting to a near uniform discharge pressure profile, significantly attenuates the total pressure distortion.
5. The last stage is effectively "throttled" by the inlet distortion even though the overall engine throttle remains unchanged. This illustrates how the last stage rotor stability margin is consumed, which makes it the limiting stage for the overall stability of the fan.
6. In general, the total temperature distortion level grows as flow passes through the fan stages. The temperature distortion at fan exit concerns the downstream core compressor and combustor as well.

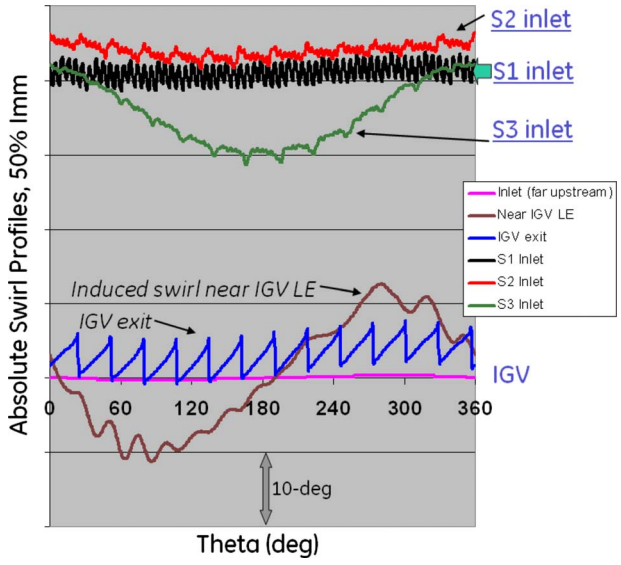

Fig. 28 Induced swirl at inlet and swirl distortion transfer of the first fan at 50% immersion

7 Future Work

In addition to the distortion simulations presented in this paper, simulations with clean inlet flow have been performed as well under the same operating conditions as reported in this paper. Analysis of fan response and the impact of inlet distortion to stability margin are being carried out, and will be reported in the future.

Acknowledgment

The authors wish to thank the support of the DoD High Performance Computing Modernization Program Office and the Aero-

Downloaded 28 May 2010 to 128.113.26.88. Redistribution subject to ASME license or copyright; see http://www.asme.org/terms/Terms_Use.cfm

nautical System Center Major Shared Resource Center for the Challenge Award that provided the high performance computing resources. Without their support, this work is not possible as it requires large number of processors and large data memory. The authors also want to thank Jenping Chen, now at Ohio State University, for his support of PTURBO; Peter Szucs and Peter Wood, both of GE Aviation, for their support of this research and many insightful discussions. Ravi Ravindranath of NAVAIR is recognized for providing early motivation to embark on this project. Mike Macrorie and Joe Capozzi from GE Aviation and Professor Garth Hobson from the Naval Postgraduate School also assisted with the simulations. The authors are grateful for the funding support provided by the Advanced Virtual Engine Test Cell (AVETeC). Finally, they thank the General Electric Co. and the Propulsion Directorate management for supporting the research and allowing the publication of this paper.

Nomenclature

PTA, PT, Pt = absolute total pressure
PS, Ps, p = static pressure
TTA, TT, Tt = absolute total temperature
TS, Ts = static temperature
θ, r, z = engine tangential, radial, and axial coordinates
b = blade chord length
u = axial velocity of the fluid
ρ = density of the fluid
s = entropy
h = enthalpy
C_p = fluid specific heat at constant pressure
ω = engine wheel speed

Subscripts

avg, ave = time average or engine circumferential average
min = minimum value in engine circumference
max = maximum value in engine circumference
local = local value at a specific immersion

References

[1] Yao, J., Gorrell, S. E., and Wadia, A. R., 2010, "High-Fidelity Numerical Analysis of Per-Rev-Type Inlet Distortion Transfer in Multistage Fans—Part I: Simulations With Selected Blade Rows," ASME J. Turbomach., **132**, p. 041014.
[2] Mazzawy, R., 1977, "Multiple Segment Parallel Compressor Model for Circumferential Flow Distortion," ASME J. Eng. Power, **99**, pp. 288–296.
[3] Yao, J., Gorrell, S. E., and Wadia, A. R., 2007. "A Time-Accurate CFD Analysis of Inlet Distortion Induced Swirl in Multistage Fans," AIAA Paper No. 2007-5059.

Downloaded 28 May 2010 to 128.113.26.88. Redistribution subject to ASME license or copyright; see http://www.asme.org/terms/Terms_Use.cfm